Effect of Ni substitution on structural, dielectric and magnetic properties of Zn ferrite nanoparticles

G. Pratibha [a], A. Thirupathi [b], V. K. Vamsi Krishna [b], P. Siva Kumar [b,*], G. K Siva Sankara Yadav [c]
[a] *Dept. of Physics, CMR College of Engineering and technology, Secunderabad, T.S.- 501401, India*
[b] *Department of Physics, Malla Reddy Engineering College (Autonomous), Secunderabad, T.S.-500100, India*
[c] *Department of physics, Rayalaseema University, Kurnool, A.P, India*

Effect of Ni doping on $ZnFe_2O_4$ samples was prepared by a sol-gel auto-combustion method. The obtained samples were calcinated at 600^0C. Then, the samples were characterized by powder X-ray diffraction, scanning electron microscopy, energy dispersive X-ray analysis, dielectric and magnetic properties. XRD results confirm the formation of a cubic spinel-type structure with an average crystallite size decreased with Ni concentration from 33.68 to 31 nm. Lattice parameter decreases with increasing Ni concentration, due to the small ionic radius of the Ni^{2+} ion. The SEM images show the morphology of the samples as spherical shaped particles in agglomeration. The dielectric constant and magnetization showed an increasing trend with increasing Ni concentration due to the rearrangement of cations at tetrahedral and octahedral sites.

(Received March 17, 2021; Accepted July 2, 2021)

Keywords: Sol-gel auto combustion, LCR, VSM and dielectric constant

1. Introduction

$NiFe_2O_4$ is the vital ferrite, commonly studied due to its implementation in many areas such as ferrofluids, catalysts, microwave devices, gas sensors, magnetic materials. The properties of ferrites depend on the nature of the charges and metal ion distribution. However, nickel ferrite posses ferromagnetism originating from the magnetic dipole moments of anti-parallel spins between Fe^{3+} ions of A sites and Ni^{2+} ions of B sites [1]. Both Ni and Zn ferrites are known to have a dominant preference for tetrahedral and octahedral locations, whereas nickel ferrite is an inverse spinel ferrite and zinc ferrite is a normal spinel ferrite. The composite Ni – Zn ferrites, however, are known to exist as a completely mixed spinel structure. The variation of elemental composition in these ferrites results in the redistribution of metal ions over the tetrahedral and octahedral sites, which can alter the properties of ferrites. The properties of these ferrite nanoparticles can also be tailored by altering parameters such as doping concentration or the synthesis process [2].

Nickel ferrite has been intensively examined as one of the magnetic nanomaterials. Nickel ferrite ($NiFe_2O_4$) has an inverse spinel structure. The position of the divalent cations (Ni^{2+}) in the crystal structure is closely related to the magnetic properties of the nickel ferrite. However, nickel ferrite posses super-paramagnetic behaviour and it has numerous applications such as gas-sensor, magnetic fluids, catalysts, magnetic storage systems, photo magnetic materials, magnetic resonance imaging, site-specific drug delivery and microwave devices[3, 4].

In this work, the dopant Ni in the $ZnFeO_4$ system is varied from 0.2 to 0.8M% and is prepared by sol-gel auto combustion method. The structural parameters such as crystallite size, lattice parameters, dielectric and magnetic properties were analyzed, and the influence of Ni on the same was explained

* Corresponding author: sivakumar.pendyala@gmail.com

2. Experimental

The chemical formula of considered Ni-doped Zn ferrite is $Ni_xZn_{1-x}Fe_2O_4$ ($0.2 \leq x \leq 0.8$) was prepared using the sol-gel auto combustion method. All used precursors are nitrates provided by Merck and Sigma Aldrich chemicals with AR grade having 99.5% purity. Nickel nitrate [$Ni(NO_3)_2$ $6H_2O$], zinc nitrate [$Zn(NO_3)_2$ $6H_2O$], ferrous nitrate [$Fe(NO_3)_3$ $9H_2O$] are precursors and citric acid [$C_6H_8O_7$ H_2O] act as burning agent and ammonia solution (NH_3) is for maintaining the pH level of solution. The nitrates were dissolved using distilled water separately in a glass beaker. They were mixed into a large beaker using magnetic stirrer after the individual chemicals had been fully dissolved. After some time a clear solution was formed, maintain citric acid to nitrate ratio as 1:3 by adding two solutions. From the previous works of literature, we consider 1:3 molar ratio is suitable for obtaining less agglomeration and tiny sized particles. Maintaining pH value equal to 7 by adding ammonia (NH_3) drop by drop under constant stirring. The previous works of literature also indicate that the size of the particles depends on the pH value. After a few hours, during the stirring and heating stage observed the homogenous solution. By continuous heating and stirring at 150°C, water molecules evaporated continuously after some time a dense and extremely sticky gel was found.

This gel was heated in the temperature range180^0C-220^0C. After some time, evapourate the water molecules completely, at the time of instant observe the burning of gel automatically give rise to auto combustion, it is very quick due to the evolution of gaseous products. Moreover, after a while, the full gel transformed to ashes or smouldered, "erupting like a volcano from the lower of the beaker to the upper. This process was completed in no moment. The obtained powders colures in dark brown ash were produced at temperature 250^0C in the form of a tree structure. Finally, the powder was cooled to room temperature. The complete preparation steps are shown in Fig. 3.2. The agate mortar is used to grind the powder for 30 minutes, then samples are obtained in the form of incredible dense. These specimens were finally calcinated under standard circumstances at 600^0C for about 4 hours and maintain room temperature.

Also, all prepared powder samples are tested for structural analyses, using XRD, SEM, FTIR and EDS techniques. Similarly, the electrical and magnetic properties studied with LCR and VSM instruments.

3. Results and discussion

3.1. Structural analysis

Fig. 1 illustrates the XRD pattern of synthesized $Ni_xZn_{1-x}Fe_2O_4$ ($0.2 \leq x \leq 0.8$) nano ferrites calcinated at 600^0C respectively. The XRD patterns of Ni-doped Zn ferrites show eight peaks situated in a range of 20˚ to 80˚ angle. The peak intensity equivalent to a structure is displayed in terms of % of miller indices as shown in fig(1). The obtained Xray diffraction information suitable with JCPDS card no.10-325. There was a change in the Zn ferrite structure with the addition of Ni content [5].

The patterns of all the samples can be indexed as a pure cubic spinel structure and found to the presence of secondary phases. The doping of Ni content from x= 0.2 to 0.8, extra peaks arises corresponding to the nickel composition as indicating with the "♦" symbol is shown in Fig. 1. The average crystallite size (D) of $Ni_xZn_{1-x}Fe_2O_4$ ($0.2 \leq x \leq 0.8$) samples were calculated by using the Debye-Scherrer eq (1)

$$D = \frac{0.9\lambda}{\beta COS\theta} \quad (1)$$

where k= 0.9 is Scherrer's constant, λ = 1.5406 A^0 is the wavelength of the incident x-rays, β is the full width at half maximum (FWHM) of diffraction peak, and θ is the Bragg's angle of diffraction. With the addition of Ni doping concentration from x = 0.2 to 0.8, the crystallite size

has changed from 33.68 to 31.29 nm at 600^0C as shown in Fig. 2. The decreasing nature of crystallite size with increasing Ni concentration below x<0.6 is due to small ionic radii of Ni^{2+} 0.74 Å replaces the larger ionic radii of Zn^{2+} 0.87Å sites [6]. But above x>0.6 crystallite size increases with doping concentration due that, Ni atoms replace the octahedral sites of Fe^{3+} ions [2,7] as shown in Fig. 2.

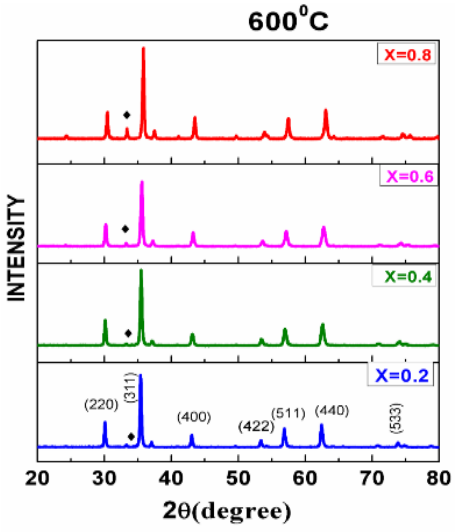

Fig. 1. XRD patteren of $Ni_xZn_{1-x}Fe_2O_4$ ($0.2 \leq x \leq 0.8$) nano ferrites calcinated at 600^0C respectively.

The decreasing nature of lattice parameter values in Ni-doped Zn ferrites samples is due to the less ionic radii of Ni^{2+} 0.78 Å substituted large ionic radii of Zn^{2+} 0.83 Å at tetrahedral sites, as shown in Fig. 2. A similar type of behaviour was observed by Ashok Kumar in nickel Zinc ferrites [8]. The lattice parameter "a" for all nickel doped Zn samples were calculated using equation (2).

$$a = d\sqrt{h^2 + k^2 + l^2} \tag{2}$$

The observed values of Crystallite Size and Lattice parameter values are listed in Table 1.

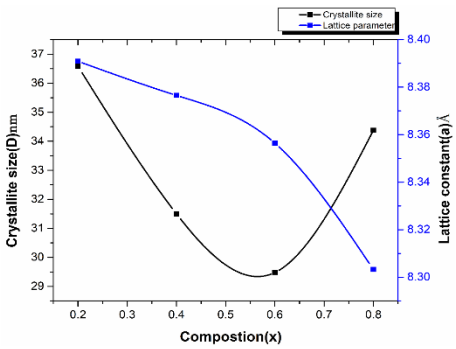

Fig. 2. Variation of crystallite size(D) and Lattice parameter(a) with Ni doping concentration.

Table. 1. Dependence of crystallite size(D), lattice constant (a) on $Ni_xZn_{1-x}Fe_2O_4$ ($0.2 \leq x \leq 0.8$) nano ferrites.

S.no	Composition (X)	Crystallite size (D) nm	Lattice constant (a) Å
1	0.2	33.68	8.390887401
2	0.4	28.01	8.376543923
3	0.6	26.6075	8.356431287
4	0.8	31.29	8.303220516

3.2 Sem analysis

The SEM analysis is used to study the morphology of all the samples. Fig. 3 shows SEM micrographs of $Ni_xZn_{1-x}Fe_2O_4$ specimens. All micrographs showed different magnifications. From the SEM images, it can be found that synthesized samples contain nanoparticles. Hence, the prepared nanoparticles look like spherical, dispersed and less agglomeration. From SEM study, the observations on grain size reveal that decreasing nature with increasing of Ni^{2+} doping concentration and changed slightly from the XRD analysis.

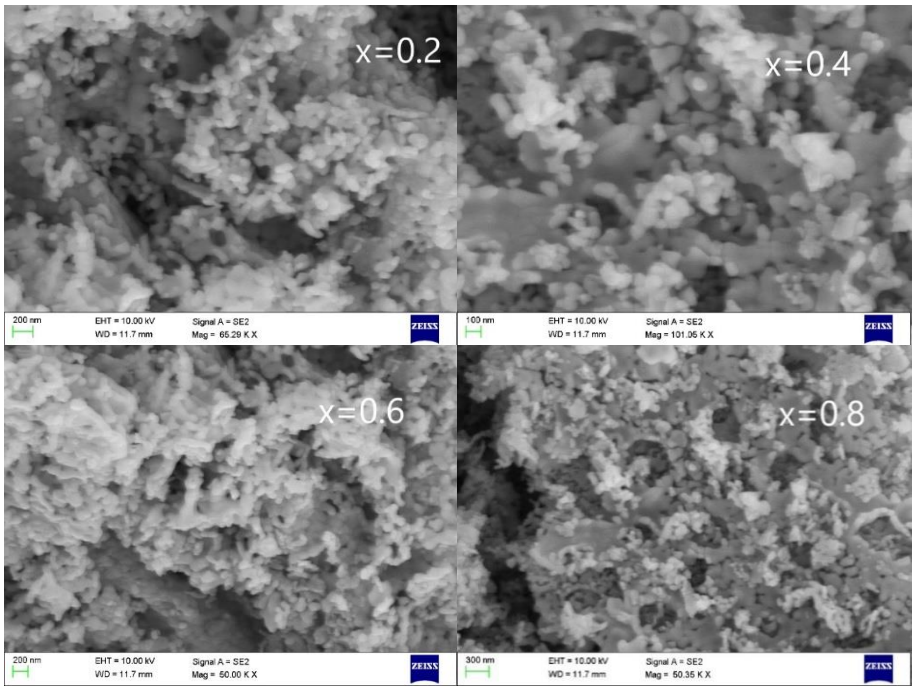

Fig. 3. SEM images for $Ni_xZn_{1-x}Fe_2O_4$($0.2 \leq x \leq 0.8$) nano ferrites.

3.3. EDS Analysis

Fig. 4 shows EDS spectrum for $Ni_xZn_{1-x}Fe_2O_4$ ($0.2 \leq x \leq 0.8$) nano ferrite samples. EDS is one of the powerful tools for describing the percentage of elemental composition in the sample. Table (2) shows the list of elemental and atomic percentages of samples. All images indicate the presence of elements used for synthesizing such as atoms of Ni, Zn, Fe, and oxygen. No other impurity components present in the samples except for these elements, so that prepared samples are defect-free and homogenous.

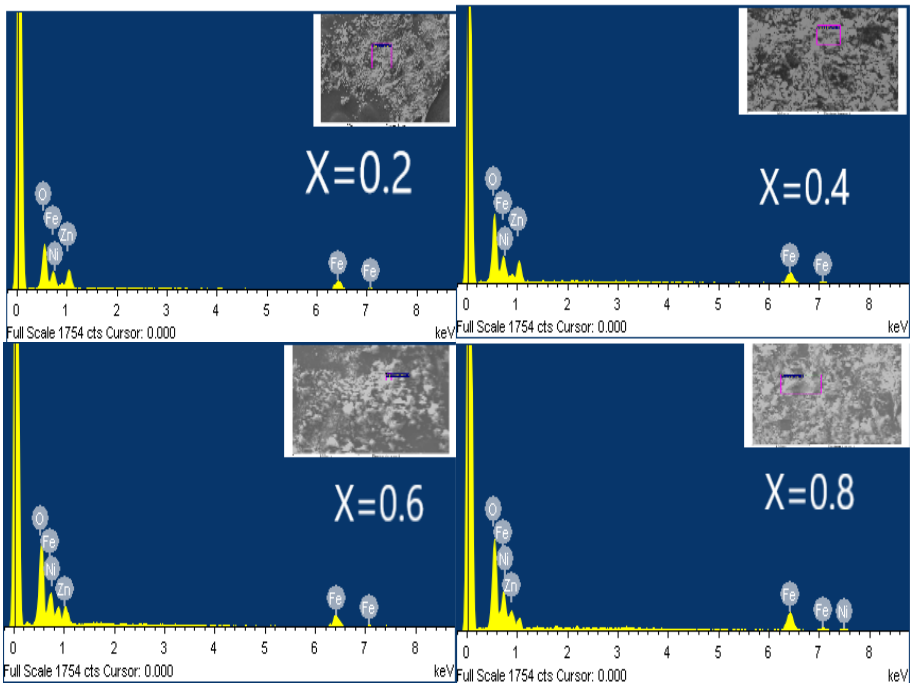

Fig. 4. The EDS pattern of $Ni_xZn_{1-x}Fe_2O_4(0.2 \leq x \leq 0.8)$ nano ferrites.

Table 2. Elemental and atomic percentages of $Ni_xZn_{1-x}Fe_2O_4$ $(0.2 \leq x \leq 0.8)$.

Element	**O**		**Ni**		**Zn**		**Fe**	
Concentration (x)	**Element %**	**Atomic %**	**Element %**	**Atomic %**	**Element %**	**Atomic %**	**Element %**	**Atomic %**
0.2	26.06	56.24	7.54	4.43	19.18	10.13	47.22	29.19
0.4	26.79	57.06	9.35	5.43	16.35	8.52	47.51	28.99
0.6	26.24	56.25	13.26	6.62	11.62	6.1	45	27.64
0.8	26.61	56.51	18.37	10.63	7.09	3.68	47.93	29.17

3.4 Dielectric properties

3.4.1. Dielectric constant

The behaviour of dielectric constant (K) with ln(f) in the frequency range 1Hz to 1MHz for $Ni_xZn_{1-x}Fe_2O_4$ $(0.2 \leq x \leq 0.8)$ calcined at 600^0C as shown in Fig. 5. The dielectric constant (K) of Ni-doped Zn ferrite at 300k has been measured by using the equation (3). All the samples are sintered at 700^0C. The values of dielectric constant (K) decrease with increasing the frequency. At a certain frequency, the observed dielectric constant is unchanged and independent of frequency, possess normal behaviour of ferromagnetic material.

$$K = C\, d / \varepsilon_o\, A \quad (3)$$

K----- is dielectric constant
d------ thickness of the sample
A----- Area of the sample
C------ capacitance of a capacitor with a dielectric

3.4.2. Effect of frequency on dielectric constant:

The dielectric constant (K) described based on the Maxwell–Wagner type of interfacial polarization that has an adequate agreement with Koop's theory. Ferrites comprise of conducting grain with weak grain boundaries. Initially, the electrons follow the applied field and piled up at the grain boundaries through the exchange mechanism that forms polarization. However, at a specific frequency, the hopping of electrons between Fe^{2+}/Fe^{3+} ions can not follow the field, and it consumes a definite time to align in the field direction that triggers to reduce the polarization. Hence the dielectric constant decreases[9,10].

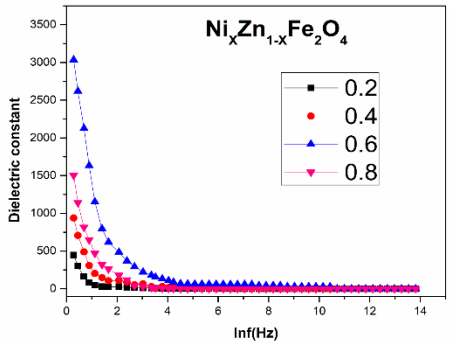

Fig. 5. Variation of dielectric constant with frequency for Ni-doped Zn ferrite nanoparticles (0.2≤ x ≤ 0.8) at 600^{0}C calcination temperature.

3.4.3. Effect of doping concentration on dielectric constant

Fig 5 shows an abrupt decrease in values of dielectric constant (k) at a low frequency and remains constant at a higher frequency. At lower frequencies, the sample x=0.2 possess a high value of dielectric constant compared to the other samples. But the behaviour of all the samples remains the same, even with an increase of Ni^{2+} concentration. The high dielectric constant (K) for all samples ($0.2 \leq x \leq 0.8$) is related to space charge polarization at grain boundaries and inhomogeneous dielectric structure. These inhomogeneities arise from preparation techniques, sintering temperature, impurities, grain structure and pores [11,12]. The reduction in dielectric constant with increasing Ni^{2+} concentration is most probable with occupancy of Ni^{2+} ions in place of Fe^{3+} ions in octahedral sites, this situation may be happened due to Ni^{2+} ion size is more compared to Fe^{3+}ions, and also dielectric constant depends on the number of ferrous ions, which take a part in electron exchange interaction. Hence, the dielectric constant decreases [12].

3.5. Magnetic properties

$NiFe_2O_4$ is the vital ferrite, commonly studied due to its implementation in many areas such as ferrofluids, catalysts, microwave devices, gas sensors, magnetic materials. The properties of ferrites depend on the nature of the charges and metal ion distribution. However, nickel ferrite posses ferromagnetism originating from the magnetic dipole moments of anti-parallel spins between Fe^{3+} ions of A sites and Ni^{2+} ions of B sites [13]. Both Ni and Zn ferrites are known to have a dominant preference for tetrahedral and octahedral locations, whereas nickel ferrite is an inverse spinel ferrite and zinc ferrite is a normal spinel ferrite. The composite Ni – Zn ferrites,

however, are known to exist as a completely mixed spinel structure. The variation of elemental composition in these ferrites results in the redistribution of metal ions over the tetrahedral and octahedral sites, which can alter the properties of ferrites. The properties of these ferrite nanoparticles can also be tailored by altering parameters such as doping concentration or the synthesis process [2].

Fig. 6 indicates the M-H curves of $Ni_xZn_{1-x}Fe_2O_4$ ($0.2 \leq x \leq 0.8$) samples at room temperature were analyzed using a vibrating sample magnetometer with a maximum field of ± 15 (kOe) at 400^0C. The derived values of saturation magnetization (Ms), residual magnetization (M_r) and coercivity (H_c) are mentioned in table 6.5. The saturation magnetization increases with increasing Ni^{2+} concentration up to x=0.6 then decrease at x=0.8. According to Neel's ferrimagnetic model, saturation magnetization can be expressed as $M_s = M_B - M_A$, where M_A and M_B are the magnetizations of A and B sites, respectively[14, 15]. With the increase in Ni^{2+} concentration, the magnetization increased and its value reached a maximum at Ni content of x=0.6 (Ms =61.077emu/g). Further, the increase of Ni^{2+} ion concentration saturation magnetization (M_s) value decreases at x=0.8 sample. This is maybe due to that occurrence of spin canting and weakening of Fe^{3+}(A)–Fe^{3+}(B) interactions at the surface of the nanoparticles [16].

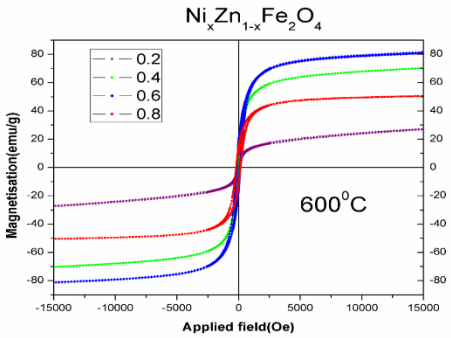

Fig. 6. M-H Curve for Ni-doped Zn ferrite nanoparticles (0.2≤ x ≤ 0.8) at 600^0C calcination temperature.

The sample $Ni_{0.2}Zn_{0.8}Fe_2O_4$ with lesser Ni concentration (x=0.2) showed superparamagnetic behaviour and (M_s) value is very less. Also, Ni ions prefer occupation of B-sites, as a result, less number of Fe ions are transferred into B-site. So that total magnetic moment is less. Whereas continuously increasing the Ni^{2+} ions in the place of Zn^{2+}, saturation magnetization (M_s) increases due to the larger magnetic moment of nickel ion as compared to zinc ions [17,18]. The magnetization in ferrites depends on so many factors like cation distribution, the existence of surface spin, etc. The cation distribution of Ni–Zn ferrites is given by [Zn^{2+}_{1-x} Fe_{1+x}^{3+}]A [$Ni_x^{2+}Fe_{1-x}^{3+}$]B [5] .

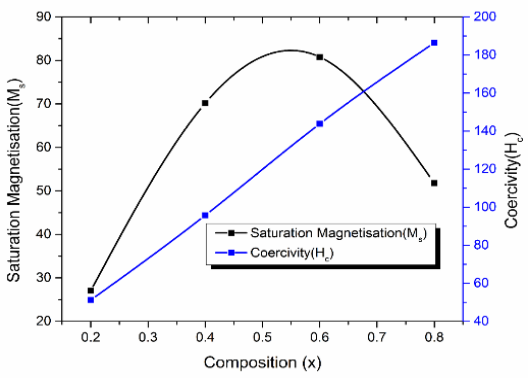

Fig. 7. Variation of saturation magnetization and coercivity for Ni-doped Zn ferrite nanoparticles

($0.2 \leq x \leq 0.8$) at 600^0C calcination temperature.

Table. 3. Dependence of Saturation Magnetisation (M_s), Coercivity(H_c) on $Ni_xZn_{1-x}Fe_2O_4$ ($0.2 \leq x \leq 0.8$) nano ferrites.

S.no	Composition(x)	Saturation Magnetisation (M_s)	Coercivity(H_c)
1	0.2	27.04	51.25
2	0.4	70.18	95.79
3	0.6	80.79	143.84
4	0.8	50.5	186.46

4. Conclusions

Nanostructured Ni-doped Zn samples have been successfully prepared with Sol-gel auto combustion method. The XRD results, confirms the formation of single-phase cubic spinel structure. The crystallite size and Lattice constant decreases with increasing Ni doping concentration.SEM micrographs reveal that all nanoparticles are looks well agglomerated with the spherical shape. EDAX analyses confirm the no foreign element present in the samples. The dielectric constant of all the samples decreases with an increase of frequency doping concentration causes to decrease in the electron exchange interaction. The maximum dielectric constant of 3000 at 0.6mol% doping concentration. From magnetic studies, the saturation magnetization increases with the increase of Ni doping concentration because Ni replaces the Zn ion, where Ni is a magnetic atom and Zn is the non-magnetic atom, which is useful for applications in the range of high frequency especially in deflection yoke rings, microwave devices and drugs delivery applications.

Acknowledgements

The author greatly indebted to Authors are thankful to *Dr Panthagani Raju*, Department of Physics, Osmania University, Hyderabad, India, for his support to carry out the LCR measurements.

References

[1] Dong-Yun Li, Yu-Kun Sun, Peng-Zhao Gao, Xiao-Liang Zhang, Hong-Liang Ge, Ceramics International **40**,16529 (2014).
[2] A. AbuEl-Fadl, A. M. Hassan, M. H. Mahmoud, TetianaTatarchuk, I. P.Yaremiy, A. M. Gismelssed, M. A. Ahmed, Journal of Magnetism and Magnetic Materials **471**, 192 (2019).
[3] E. Harmony, J. Depeyrot, M. H. Sousa, F. A. Tourinho, J. C. Bacri, R. Perzynski, Y. L. Raikher, I. Rosenman, J. Appl. Phys. **88**, 6628 (2000).
[4] Y. L. Raikher, V. I. Stepanov, J. Depeyrot, M. H. Sousa, F. A. Tourinho, E. Hasmonay, R. Perzynski, J. Appl. Phys. **96,** 5226 (2004).
[5] A. D. Sheikh, Æ V. L. Mathe, J. Mater. Sci. **43**, 2018 (2008).
[6] M. Zhijun, Change Mang, Xingyuan Weng, Qi Zhang, Liwei Si, Haitao Zhao, Materials **11**(4), 590 (2018).
[7] Ashok Kumar, Annveer, Manju Arora, M. S. Yadav, R. P. Panta, Physics Procedia **9**, 20 (2010).
[8] Ashok Kumar, Parmod Kumar, Geeta Rana, M. S. Yadav, R. P. Pant, Appl. Sci. Lett. **1**(2), 33 (2015).
[9] K. W. Wagner, Ann. Phys. **40**, 817 (1913).

[10] C. G.Koops, Phys. Rev. **83**(1), 121 (1951).
[11] A. Sutka, M. Stingaciu, G. Mezinskis, Journal of Materials Science **47**(6), 2856 (2012).
[12] R. C. Kambale, N. R. Adhate, B. K. Chougule, Journal of Alloys and compounds **491**(1-2), 372 (2010).
[13] Dong-Yun Li, Yu-Kun Sun, Peng-Zhao Gao, Xiao-Liang Zhang, Hong-Liang Ge, Ceramics International **40**, 16529 (2014).
[14] M. Sertkol, Y. Köseoğlu, A. Baykal, H .Kavas, A. Bozkurt, M. S. Toprak, Journal of Alloys and Compounds **486**, 325 (2009).
[15] T. R. Tatarchuk, N. D.Paliychuk, M. Bououdina, B. Al-Najar, M. Pacia, W. Macyk, A. Shyichuk, Journal of Alloy and Compd. **731,** 1256 (2018).
[16] M. Atif, M. Nadeem, J. Sol-Gel Sci. Technol. **72**, 615 (2014).
[17] K. H. Wu, Mater. Res. Bull. **40**, 2080 (2005).
[18] K. B. Modiet, Indian, J. Pure & Appl. Phys. **34**, 92 (1996).